

Reconfigurable quantum fluid molecules of bound states in the continuum

Antonio Gianfrate,¹ Helgi Sigurðsson,^{2,3,*} Vincenzo Ardizzone,¹ Hai Chau Nguyen,⁴ Fabrizio Riminucci,⁵ Maria Efthymiou-Tsironi,¹ Kirk W. Baldwin,⁶ Loren N. Pfeiffer,⁶ Dimitrios Trypogeorgos,¹ Milena De Giorgi,¹ Dario Ballarini,^{1,†} Hai Son Nguyen,^{7,8} and Daniele Sanvitto¹

¹*CNR Nanotec, Institute of Nanotechnology, via Monteroni, 73100, Lecce, Italy*

²*Science Institute, University of Iceland, Dunhagi-3, IS-107 Reykjavik, Iceland*

³*Institute of Experimental Physics, Faculty of Physics, University of Warsaw, ul. Pasteura 5, PL-02-093 Warsaw, Poland*

⁴*Naturwissenschaftlich-Technische Fakultät, Universität Siegen, Walter-Flex-Straße 3, 57068 Siegen, Germany*

⁵*Molecular Foundry, Lawrence Berkeley National Laboratory, One Cyclotron Road, Berkeley, California, 94720, USA*

⁶*PRISM, Princeton Institute for the Science and Technology of Materials, Princeton University, Princeton, New Jersey 08540, USA*

⁷*Univ Lyon, Ecole Centrale de Lyon, INSA Lyon, Université Claude Bernard Lyon 1, CPE Lyon, CNRS, INL, UMR5270, Ecully 69130, France*

⁸*Institut Universitaire de France (IUF), 75231 Paris, France*

(Dated: August 2, 2024)

Topological bound states in the continuum are confined wave-mechanical objects that offer advantageous ways to enhance light-matter interactions in compact photonic devices. In particular, their large quality factor in the strong-coupling regime has recently enabled the demonstration of Bose-Einstein condensation of bound-state-in-the-continuum polaritons. Here, we show that condensation into a negative-mass bound state in the continuum exhibits interaction-induced state confinement, opening opportunities for optically reprogrammable molecular arrays of quantum fluids of light. We exploit this optical trapping mechanism to demonstrate that such molecular complexes show hybridization with macroscopic modes with unusual topological charge multiplicity. Additionally, we demonstrate the scalability of our technique by constructing extended mono- and diatomic chains of bound-state-in-the-continuum polariton fluids that display non-Hermitian band formation and the opening of a minigap. Our findings offer insights into large-scale, reprogrammable, driven, dissipative many-body systems in the strong-coupling regime.

I. INTRODUCTION

Development of artificially structured materials at the nanoscale in solid-state technologies and photonics has opened opportunities to explore the coupling between matter and confined light. In the recent years, confined photonic modes—known as symmetry protected bound states in the continuum (BICs)—have emerged in full force through precise parameter tuning in synthetic lattices across various wave-mechanical and quantum systems [1]. In optical systems [2], these extremely high Q -factor BIC resonances cannot radiate energy despite residing within the light cone, opening perspectives on ultralow threshold lasing devices emitting coherent vectorial light [3, 4] associated with the inherent momentum-space topological charge of BICs [5, 6]. Aside from low-threshold lasing devices, photonic BICs have a wide reaching application from plasmonics to photonic waveguides and crystals including sensing [7], filtering [8], and enhancing light-matter interactions [9]. Other interesting optical effects like multistability [10] and solitons [11] have been predicted for BICs when nonlinearity is introduced to the system.

Quite recently, BICs operating in the strong light-matter coupling regime in subwavelength grating semiconductor heterostructures were proposed [12] and demonstrated [13, 14]. In these structures emergent light-matter bosonic quasiparticles known as exciton-polaritons (here after polaritons) can undergo nonequilibrium Bose-Einstein condensation [15] in a low-loss BIC mode [16].

Polaritons are formed due to the strong coupling of light (photons) and matter (excitons) in semiconductor cavities with embedded quantum wells [17]. The photonic component gives polaritons extremely small effective mass, whereas the exciton component makes them highly interactive [18]. Upon condensation, the macroscopic polariton wavefunction is explicitly encoded in the spontaneous coherent emission of photons from the cavity, giving direct access to all of its degrees of freedom through standard optical techniques. Various phenomena associated with other branches of physics have now been demonstrated in polariton condensates including topological insulators [19], quantized vorticity and superfluidity [20], spontaneous phase [21, 22] as well as pseudospin-pattern formation [23], and much more.

Considerable effort in contemporary photonics has been dedicated to designing tailored polariton potential landscapes [24] for simulation of exotic Hamiltonians [25] and possibly unconventional computing purposes [26].

* helg@hi.is

† dario.ballarini@nanotec.cnr.it

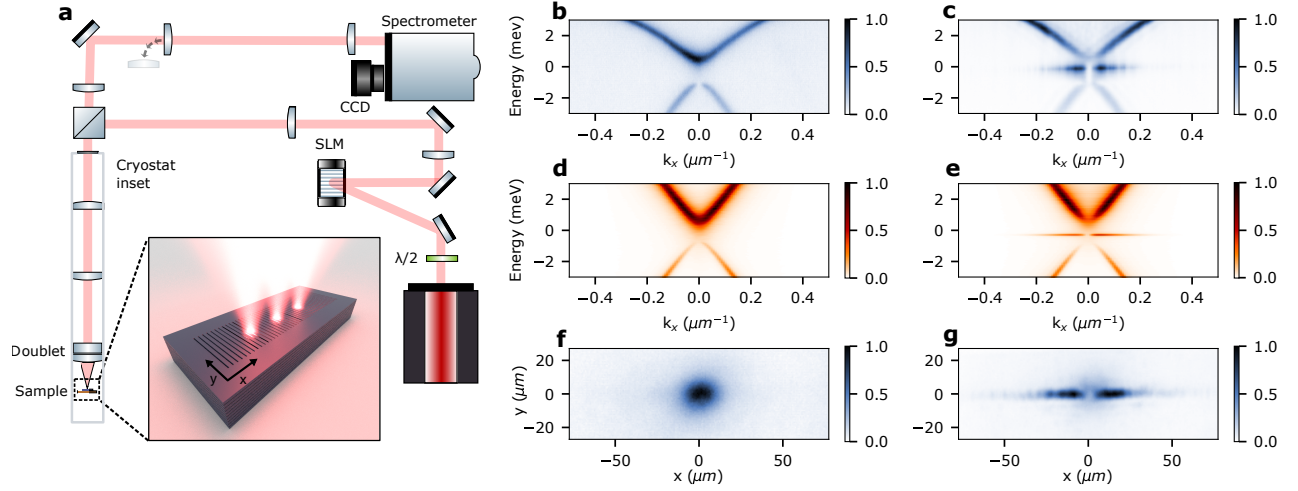


Figure 1. **The exciton-polariton BIC condensate in a quantum-well grating waveguide:** (a) Schematic of the experimental setup. In the excitation line the surface of the spatial light modulator (SLM) is recreated in the Fourier plane of the excitation objective. According to the requirements of the particular experiment, the sample's luminescence is captured by a 2f detection line, and either the real or Fourier plane is reconstructed on the monochromator entrance. The inset is an artistic representation of the grating waveguide sample. (b),(c) Experimental energy momentum dispersion crosscut along $k_y = 0$ below and above condensation threshold, respectively. (d),(e) Corresponding calculated dispersions using a Dirac equation (see Eq. (1) and Methods). Energy scales are shifted with respect to the energy of the gap state in (c). (f),(g) Corresponding measured real space distribution of the emission.

The engineered potential typically stems from irreversible techniques, requiring new samples for different tasks, based on e.g., etching [27], patterning mesas [28] or polymer layers [29], or metallic deposition [30] on the microcavity surface. Alternatively, structured nonresonant excitation beams acting on the exciton component of the polariton have the advantage of being fully reversible giving also the possibility of dynamical fast modification of the potential landscape. The nonresonant beam photoexcites a co-localized reservoir of hot excitons which locally amplify and blueshift polaritons [31], underpinning the phenomena of ballistically coupled polariton Bose-Einstein condensates [32], optical trapping [33, 34], and all-optical polariton lattices [32, 35, 36]. When the beam is removed, the reservoir rapidly decays and, subsequently, so does the pump-induced polariton potential, underlining the reprogrammable feature of the system.

For conventional cavity polaritons with positive effective mass the pump-induced localized blueshift means that outside of the pump region condensate polaritons can convert elastically into states with high k -vectors with subsequent fast expansion velocities. This means that polaritons are always repelled from their gain region, increasing the condensate threshold power and lowering its coherence time. The contrary, an excitation profile which provides effective local redshift would form an attractive potential in the gain region. This implies that polaritons can be optically confined while still being efficiently pumped, a scheme that has not been explored properly up to date.

Here, we empower this new paradigm by using nega-

tive mass BIC polaritons in subwavelength quantum-well waveguide gratings [16]. Until now, the negative mass scheme has primarily been explored in polaritonics using micropillar arrays [37, 38] with several fundamental differences to our BIC platform. First, our waveguide approach overcomes a geometric limitation of the micropillars, enabling sub-micrometer patterning without the exciton quenching issues. Second, the diffracting coupling mechanism and losses between polaritonic branches and the continuum can be engineered giving control over the BIC properties and non-trivial topology.

In this work we demonstrate how BIC polariton condensates allow us to optically and reversibly structure macroscopically coherent nonlinear fluids of light to simulate molecular bonding between different optical traps. We provide experimental realization of coherent quantum mode hybridization in a BIC condensate dyad (two pump spots) similar to a bosonic Josephson junction, Bloch band formation in an artificial mono-atomic quasi-1D chain (ten spots), and subband formation with celebrated minigap opening in staggered chains analogous to the Su-Schrieffer-Heeger (SSH) model. Our results are the first evidence of using nonlinearly spatially-localized BICs to design extended evanescently coupled many-body systems that preserve the vectorial momentum-space topological textures. Interestingly, our results can be approximately described with a massive non-Hermitian Dirac model due to the linear dispersion of waveguided photons opening a new pathway in exploring synthetic many-body Dirac Hamiltonians in the strong light-matter coupling regime. Furthermore adding nonlinearities to BICs we

show that it leads to surprisingly effective spatial confinement of these very long-lived states. This is in sharp contrast with the conventional BICs in photonic lattices, which are delocalized states at least along one dimension [1].

II. RESULTS

A. Single trapped BIC condensate

Our sample consists of a planar semiconductor waveguide with a grating along the x -direction and embedded GaAs-based quantum wells (see Fig. 1a and Methods). The presence of the grating folds the guided photonic modes lying outside the light cone across $k_x = 0$ [12]. An anticrossing occurs due to finite non-Hermitian coupling between counterpropagating modes through the radiative continuum with a gap opening at the Γ -point, directly tunable through the grating filling factor and etching depth [39]. By tuning the phase of this complex-valued coupling it is possible to entirely suppress the losses for one of the photonic eigenstates at the Γ -point, corresponding to a symmetry protected BIC. In our case, the BIC is located in the lower energy branch (see Fig. 1b). Namely, the two counter-propagating polariton guided modes are coupled via the gratings (i.e. diffractive coupling) and also via the radiative continuum (i.e. radiative coupling). The effects of these coupling is two-fold: i) gap opening with two polaritonic branches, and ii) destructive interference of radiative losses for the lower polariton branch at the normal incidence, leading to a nodal line in the far-field emission.

As the quantum well excitons become strongly coupled with the guided photons, the resultant polaritons inherit the BIC state from the photons and strong interparticle Coulomb interactions from the excitons. The unique combination of these properties has recently enabled ultralow threshold polariton condensation under nonresonant excitation [16]. We demonstrate this effect in Fig. 1 for a single Gaussian pump spot (see Methods for details on the experiment). Figures 1b and 1d show, respectively, the measured and modeled far field photoluminescence (PL) having in-plane wavevector along the corrugation direction. This scheme excites polaritons nearly uniformly across the two dispersion branches below the exciton energy [40]. The BIC at the Γ -point of the lower branch does not radiate into the continuum, as expected, which manifests as a dark notch.

When the pump is increased above condensation threshold the emission changes dramatically (see Figs. 1c,e) [16]. The long-lifetime BIC results in enhanced amalgamation polaritons at the lower branch extremum through spontaneous scattering. At high enough powers, stimulated scattering is triggered into the BIC state where a negative effective mass polariton condensate forms. The pump induced blueshift then attracts polaritons to the spot, effectively confining the conden-

sate. This is in contrast to ballistic polariton condensates in planar cavities where most of the condensate converts into large momentum outflowing polaritons [32]. The fundamental mode of the pump-induced trap is shifted into the bandgap and is visibly occupied by polaritons as seen in Figs. 1c,e. The corresponding PL measured in real space is shown in Fig. 1g. Notice that the fundamental trap mode emits light with an odd-parity (i.e., a dark nodal line at $k_x = 0$) and that the incoherent PL in the upper branch suffers a slight depletion around $k_x \approx 0$ because of the localized pumping.

At low momentum, and for sufficiently negative exciton-photon detuning, roughly exceeding half the light-matter Rabi coupling strength, the polariton dispersion can be approximated by a simplistic single-particle model. A non-Hermitian 1D Dirac Hamiltonian describing the coupling between massless forward and backward propagating polariton modes $\psi_{F,B}$ with velocity v along the waveguide [12, 16],

$$\hat{H} = \begin{pmatrix} -i\hbar v \partial_x - i\gamma + V(x) & U + i\gamma \\ U + i\gamma & i\hbar v \partial_x - i\gamma + V(x) \end{pmatrix}. \quad (1)$$

Here, the pump induced exciton reservoir is taken as a static potential $V(x)$ because of the exciton's much heavier mass. The propagating polaritons are coupled through U coming from the periodic corrugation of the waveguide and—being folded above the light line—each of them leak to the radiate continuum with the same coupling strength γ [12] (note, we have neglected non-radiative exciton losses which are not essential in our results). The radiative channel makes it possible for a loss exchange mechanism of the same strength γ . Such an interference via radiating waves dictates the far-field emission of polariton modes and is the origin of the polariton BIC formation. In absence of the potential $V(x)$, the eigenmodes of the Hamiltonian (1) in k -space give rise to two polaritonic bands with opposite curvature $\pm v^2/2U$. These bands are separated by a gap of $2U$. The loss exchange, on the other hand, affects the mode losses, resulting in a mode with a vanishing linewidth, i.e. the BIC state, and a mode that absorbs all the radiative losses [16]. The blueshifting potential is taken to be Gaussian $V(x) = V_0 e^{-x^2/2w^2}$ of width w . When the pump is weak then $V_0 \approx 0$ and we recover the non-trapped polariton dispersion shown in Fig. 1b,d (see Methods for details on calculations). When the pump is strong ($V_0 > 0$) we see a clear mode within the bandgap in agreement with experiment corresponding to the fundamental mode of the effective confining potential $V(x)$ (see Fig. 1c,e).

B. BIC polariton molecules

To demonstrate the novel concept of our trapped condensates, we structure our excitation beam into two spatially separated spots thus creating a double trap potential or alternatively a driven-dissipative bosonic Josephson junction. This forms a very simple setting to study

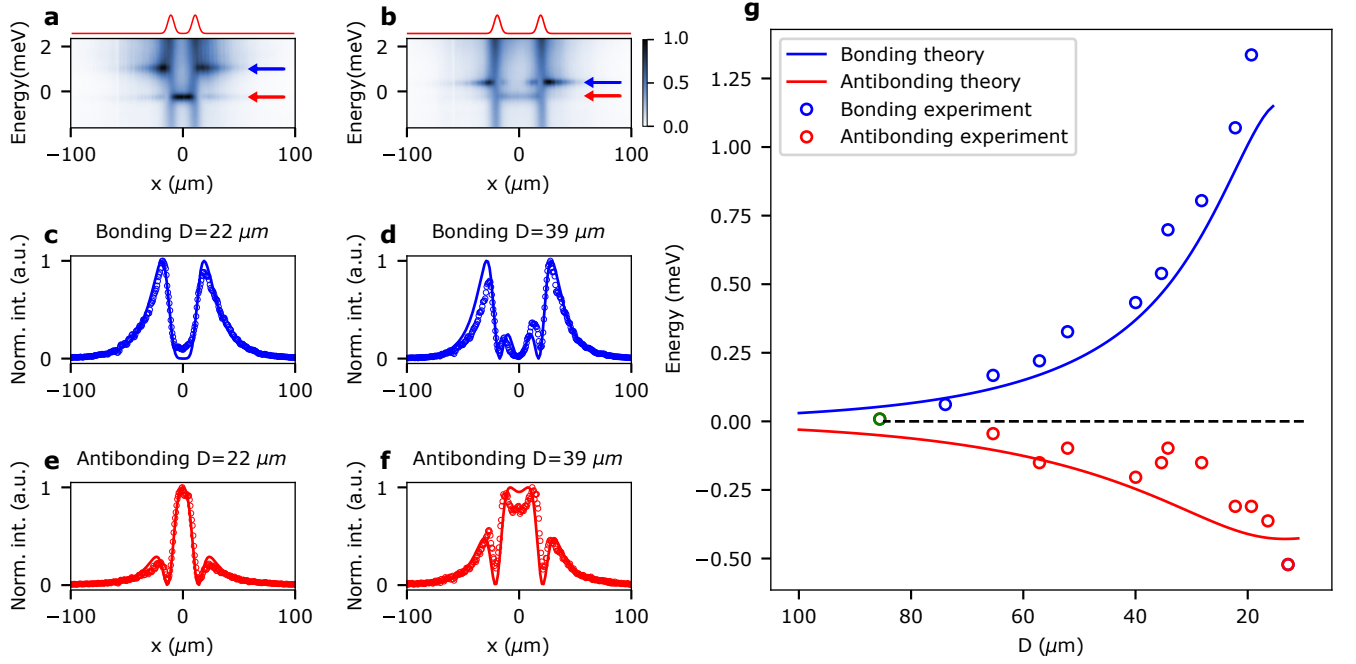


Figure 2. **BIC molecule condensate characterisation:** (a,b) Energy resolved real space PL crosscut at $y = 0$ showing the double trap case for an pump spot separation distance of 39 and 22 μm , respectively. The red lines are a scaled schematic representation showing the pump profile. (c-f) Experimental (markers) and theoretical (solid lines) mode profiles of the hybridized trapped condensates. (g) Energies of the hybridized modes as a function of pump spot separation distance for constant power. Dashed line refers to the isolated condensate energy E_0 (shifted to zero for brevity $E = \bar{E} - E_0$ with $E_0 = 1520.2 \text{ meV}$). Blue and red markers represent the upper (bonding) and lower (antibonding) mode energies and corresponding solid lines represent the energies from the Dirac model. The green marker indicates the measured energy for single trapped condensate.

fundamental quantum mechanical effects such as mode hybridization but now with added BIC topological charge structure in k -space. This is in contrast to conventional double-trap studies (i.e., no BIC) using ultracold atomic gases [41], other polariton systems [27, 42, 43] and photonic condensates [44].

The condensate energy-resolved near-field PL in the double trap is shown in Figs. 2a,b for trap separation of $D = 39$ and $22 \mu\text{m}$, respectively. Mode hybridization can be clearly observed for both cases, as the condensate starts populating the new bonding and antibonding BIC states characterized by clear normal-mode splitting. The corresponding spatial line-profile envelopes of the bonding and antibonding modes are shown in Fig. 2c,d and 2e,f with overlaid analytical modes obtained from solving the bound states of the equation (1) with $V(x)$ having the form of a double Gaussian potential, given by $V(x) = V_0 e^{-(x-D/2)^2/2w^2} + V_0 e^{-(x+D/2)^2/2w^2}$ (see Methods). Because of the characteristic of BIC, light emitted from the waveguide depicts an unconventional arrangement of nodes (corresponding to π phase jumps) in the total condensate wavefunction that are captured by our model. Differently from previous polariton schemes, we can continuously tune the evanescent inter-condensate coupling and, consequently, the energy splitting between the bonding and antibonding states by simply adjust-

ing the spot separation distance D as shown in Fig 2g. As expected, decreasing the distance between the two spots enhances the overlap between the trapped condensates, exponentially splitting the bonding and antibonding states. Interestingly, the blue-shift of the bonding state increases much faster than the red-shift of the anti-bonding one when decreasing the distance D . In particular, when $D < 16 \mu\text{m}$, trap contains only the anti-bonding state (see Fig. S1 in the Supplemental Information for details). Indeed, for small distance D , the blue shift of the bonding-state is so strong that it falls into the energy band of the structure outside the trap. These available states allow polaritons to tunnel out of the traps via the Klein tunnelling mechanism [45]. The bound state energies computed from the theoretical model (1), despite its simplicity, reproduces the measurement data to a fairly good accuracy with a single fit parameter $V_0 = 3.5 \text{ meV}$; all other parameters are fixed from experiments carried out below the condensation threshold. The far-field profiles in Figs 2c-f were then computed without any further fitting (see Methods).

In order to fully characterize the BIC molecules, we studied their topological structure by investigating the condensate momentum space polarization. BICs are characterised by topological charges [5] corresponding to polarization vortices in momentum space (Fig. S2).

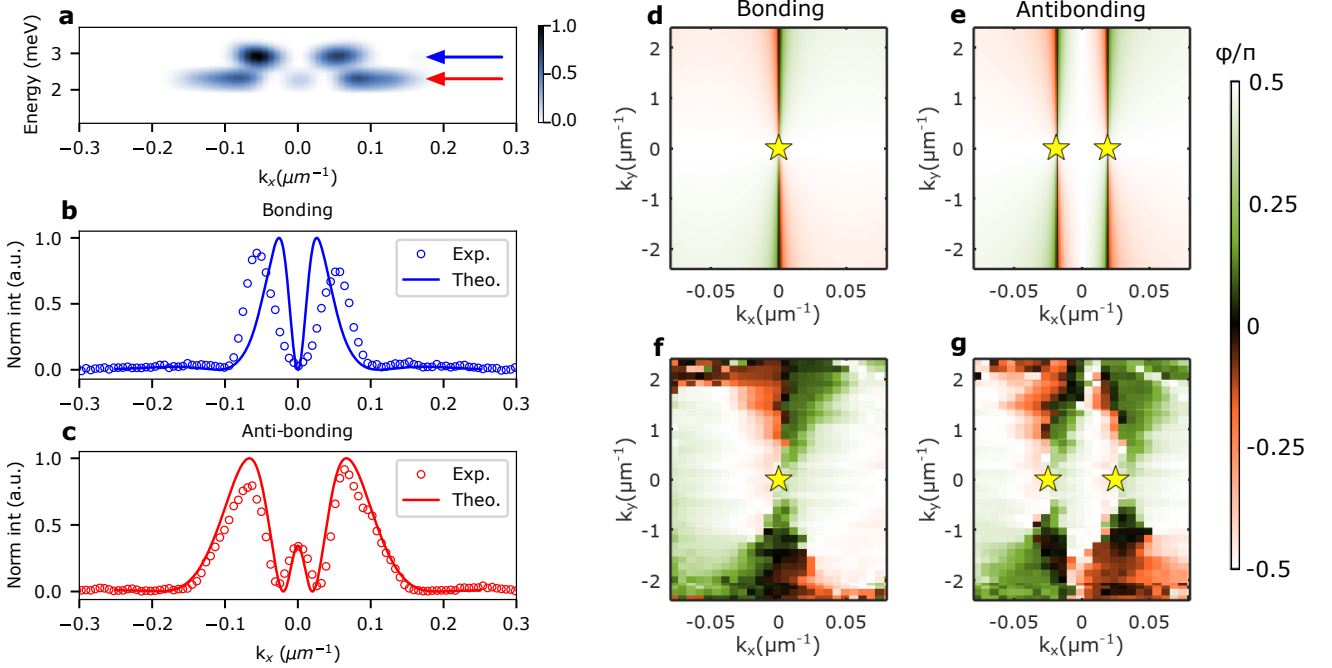


Figure 3. **Momentum space photoluminescence characteristics in the double-spot arrangement:** (a) Energy-momentum crosscut along $k_y = 0$, for a double trap potential with the pumps separated by $31\mu\text{m}$. The two arrows mark the energies of the bonding and antibonding above thresholds, i.e. for higher excitation power. Here the condensates signals results blueshifted respect to Fig 2 and no residual photoluminescence from the non condensed states can be observed. (b,c) Corresponding experimental (markers) and calculated (solid curves) PL line profiles of the two states. Calculated (d,e) and measured (f,g) momentum space distribution of the condensate polarization vector ϕ for the bonding and antibonding state, respectively.

It was recently confirmed that a single polariton BIC condensate could indeed inherit this topological structure [16]. However, there has been no investigation into the topological structure of extended BIC condensates, or BIC molecules. Figure 3a shows the energy resolved cross section of the momentum space PL showing the molecule bonding and antibonding states above threshold. The corresponding comparison between the experimental and theoretical reciprocal space line profiles are depicted in Fig. 3b,c showing good agreement. We attribute the small discrepancy in panel 3b to the dynamical/transient blueshift of the state because the experiment is performed under femtosecond pulsed excitation (see Methods and Supplemental Video 1). Here again the phase jumps can be clearly distinguished as dark nodes. Performing an energy and polarization resolved tomography we retrieved the momentum space maps of the polarization direction φ (i.e., orientation of the polarization ellipse). The polarization textures were also theoretically calculated from the eigenvectors of Dirac equation (1) (see Methods). The resulting theoretical and experimental maps for the bound and anti-bound state are shown in Fig. 3d,e and Fig. 3f,g, respectively. These maps show the presence of a single polarization vortex in the bound state and a pair of vortices in the anti-bound state. This finding underlines that each node

in the hybridized double-trap system corresponds to a polarization vortex having the same topological charge of the original photonic BIC. Therefore, the topological charge of the hybridized state has increased with respect to the modes of the uncoupled traps, a finding unreported to date.

By further increasing the complexity of the potential landscape (by increasing the number of traps), it is possible to add more and more states within the gap with alternating parity. This is clearly illustrated in Fig. S3 in the Supplemental Material which compares single, double, and triple trap configurations.

C. BIC condensate chains

Lastly, we studied the feasibility of simulating large-scale systems by coupling 10 condensates together arranged in a finite 1D chain with a lattice constant a . Figures 4a and 4b show experimental and calculated energy-resolved PL in momentum space for a regular (i.e. effectively mono-atomic) 10 spot chain extracted along the x direction. Polaritons, within their lifetime, experience the discrete translational symmetry in the bulk of the chain, giving rise to Bloch modes and associated crystalline bands, the hallmark of solid-state physics. Ap-

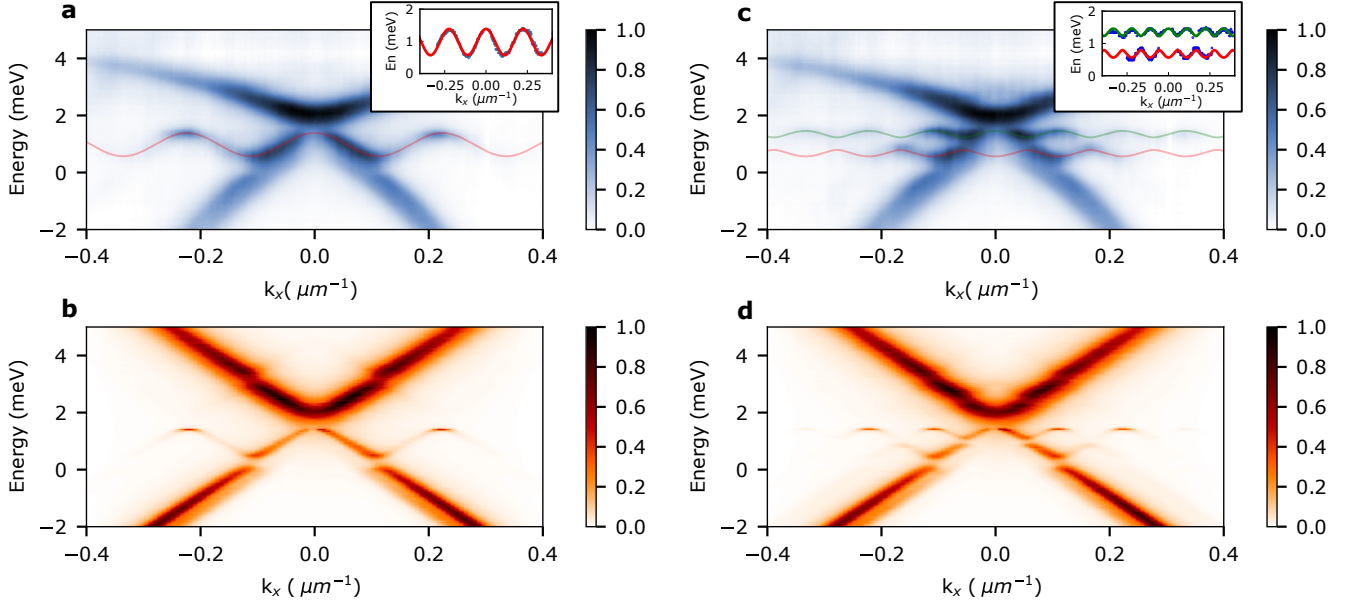


Figure 4. **10-BIC condensate chain** (a) Experimental energy momentum crosscut showing the additional band for an uniform 10 spot chain. Here the PL contribution of the exciton has been subtracted to better highlight the dispersion. Red curve shows the tight binding approximation for the s -band, $E = 2J \cos(k_x a)$. (b) Corresponding calculated dispersion using the lossy Dirac model (1). (c) Measured energy-momentum PL crosscut for a staggered lattice with a staggering contrast $a/b = 1.75$. The red and green lines depict the fitting of the SSH dispersion $E_{1,2} = \pm \sqrt{J_a^2 + J_b^2 + 2J_a J_b \cos[(a+b)k_x]}$. The inset show the resulting curves overlapped with the extracted experimental data. The fit parameters are $J_a = 0.33$, $J_b = 0.11$ meV, $a = 20 \mu\text{m}$, $b = 36 \mu\text{m}$. (d) Calculated dispersion of a staggered lattice using the parameters extracted from the measure in panel c. In this panel the energy is re-scaled to the energy of the not blueshifted BIC state as $E = \bar{E} - E_0$ with $E_0 = 1524.8$ meV.

proximating the polaritons as deeply confined in their pump-induced traps we can fit the observed Bloch band with the standard expression for mono-atomic (s -orbital) dispersion from tight-binding theory, $E = 2J \cos(k_x a)$ where J is the coupling (hopping) energy between sites (red curve in Fig. 4b with $a = 28 \mu\text{m}$ and $J = 0.2$ meV). The goodness of the fit underlines that the optically trapped polaritons here can be accurately described using tight-binding theory in contrast to coupled ballistic condensates [35] (Please refer to Fig. S3 for a direct comparison between the two mechanisms).

Another notable information that can be extracted from this experiment is related to the Bloch band topology. At $k_x = 0$ the Bloch modes inherit the same topology of the BIC mode as demonstrated by the lack of emission at the Γ -point. However for the off Γ Brillouin zones the notch is absent, as also confirmed by the numerical simulations presented in Fig. S4.

To further demonstrate the advantage of our reconfigurable all-optical lattice we show in Fig. 4(c,d) the dispersion for a staggered lattice with a contrast $a/b = 1.75$. Here, we observe the opening of a minigap as two distinct Bloch bands form, as expected from tight binding considerations. The green and red curves in Fig. 4c represent the classical dispersion for a dimer lattice $E_{1,2} = \pm \sqrt{J_a^2 + J_b^2 + 2J_a J_b \cos[(a+b)k_x]}$, with J_a and J_b the hopping coefficients and a and b the site distances.

This type of a staggered system is a polariton analogue of the SSH Hamiltonian which is perhaps one of the simplest models to possess topological nontrivial gap opening and associated protected edge states. The full characterisation of these artificial polariton lattice systems is beyond the scope of the current study. We however predict that a wealth of nonlinear phenomena such as solitons and persistent Bloch oscillations can be studied in our evanescently coupled optical lattices offering a contrasting viewpoint with respect to ballistic lattices [35] and adding an extra control-knob on the non-Hermitian character of each "monomer".

III. DISCUSSION

We have shown that it is possible to optically construct macroscopically coherent artificial molecules and atomic chains using polariton condensates in an extreme nonequilibrium setting protected from the continuum. For this purpose we have used a subwavelength grating waveguide with embedded quantum wells possessing a photonic BIC which, through strong light-matter coupling, enhances the lifetime of emergent polaritons and allows them to condense at the extremum of a negative mass dispersion around $k_x \approx 0$, opening a path to explore driven nonequilibrium negative-mass hydro-

dynamics [46]. This is in stark contrast to the $|\mathbf{k}_{\parallel}| > 0$ extrema in the so-called anomalous lower polariton dispersion which cannot display condensation [47]. Because of their strong interactions, the negative mass polaritons become self-trapped leading to efficient condensation co-localised with the pump spot.

As a result, a structured light source can reconfigurably write-in various potential landscapes that are accurately described through evanescently coupled trapped in-plane waves and tight binding models reminiscent of optical lattice for cold atoms [48]. This technique overcomes a severe challenge in realizing reprogrammable macroscopic many-body systems with continuously tunable parameters in the strong light-matter coupling regime [24] with exciting prospects for many-body polariton simulation [26] such as driven macroscopic quantum self-trapping and Josephson oscillations [43] and quantum-dissipative phase transitions in optically reconfigurable non-Hermitian tight-binding lattices [49]. Indeed, the self-trapping of our waveguided polaritons is in strong contrast to the ballistic non-trapped condensate polaritons in conventional and fabrication costly planar Bragg reflector cavities [32, 35]. Here, no sample post-processing to create potential landscapes [50] is required, and our reprogrammable optical-trapping technique efficiently stimulates polaritons in the trap (i.e., the optical gain is inside the trap) in contrast to other methods where the gain is outside the trap [36]. This constitutes a significant novelty in the solid state condensation panorama opening new possibilities in investigating complex many-body Hamiltonians in a continuously reconfigurable system like demonstrated in Fig. 2.

A remarkable observation is the increase of momentum space topological charges when two or more BIC condensates are brought together to hybridize into extended modes as shown in Fig. 3. As more condensates are added, the number of accessible topological charges in principle increases but at the cost of becoming more spread out in the far field due to the decreasing contrast between antinodal lines in the near field. This finding could lead to controllable generation of polarization vortices complementing the surging interest in utilizing optical vortices and vectorial coherent light sources for communication and information processing technologies [51].

When multiple pump spots are brought together (see Fig. 4) our system becomes described by Bloch's theorem and we gain access into non-Hermitian lattice Hamiltonians. This is particularly exciting from the perspective of being able to simulate many fundamental crystalline systems by exploiting the strong polariton interactions while at the same time being able to optically read out all the relevant dynamics. For this purpose we have demonstrated tunable transition from a mono-atomic 1D chain to the Su-Schrieffer-Heeger chain [52] in Fig. 4 with clear minigap opening and subband formation.

We have also shown that our results can be reasonably reproduced using a 1D Dirac Hamiltonian with a mass term. The Dirac Hamiltonian appears in many low

dimensional systems such as graphene, transition-metal dichalcogenides, and around the crossing of spin-bands in a Rashba Hamiltonian. It describes intriguing electron transport effects around corresponding Dirac cones giving rise to quantum Hall physics, topological phases, and Weyl semimetals. Its appearance in BIC polariton condensates holds promises for further exploration into nonlinear driven-dissipative Dirac dynamics. Recently, Dirac cones have gained a great deal of interest in photonic [53–55] and polariton systems [56, 57] to bring associative topological electron concepts into the field of topological photonics. An interesting perspective of this Dirac Hamiltonian, for a future study, is that the grating filling factor can be adjusted to change the sign of the mass parameter U [12]. This implies that an interface between two gratings with different sign of U is described by the Jackiw-Rebbi model [58–60] possessing a zero-energy midgap state.

IV. ACKNOWLEDGEMENTS

H.S. acknowledges the project No. 2022/45/P/ST3/00467 co-funded by the Polish National Science Centre and the European Union Framework Programme for Research and Innovation Horizon 2020 under the Marie Skłodowska-Curie grant agreement No. 945339; and the Icelandic Research Fund (Rannis), Grant No. 239552-051. A.G., V.A., D.T., M.D., D.B., D.S. acknowledge the Italian Ministry of University (MUR) for funding through the PRIN project “Interacting Photons in Polariton Circuits” – INPhoPOL (grant 2017P9FJBS), the project “Hardware implementation of a polariton neural network for neuromorphic computing”–Joint Bilateral Agreement CNR-RFBR (Russian Foundation for Basic Research)–Triennial Program 2021–2023, the MAECI project “Novel photonic platform for neuromorphic computing”, Joint Bilateral Project Italia-Polonia 2022-2023, PNRR MUR project: “National Quantum Science and Technology Institute”- NQSTI (PE0000023), PNRR MUR project: “Integrated Infrastructure Initiative in Photonic and Quantum Sciences” - I-PHOQS (IR0000016), and the project FISIR - C.N.R. “Tecnopolo di nanotecnologia e fotonica per la medicina di precisione” - CUP B83B17000010001 and “Progetto Tecnopolo per la Medicina di precisione, Deliberazione della Giunta Regionale n. 2117 del 21/11/2018. H.S.N is funded by the French National Research Agency (ANR) under the project POPEYE (ANR-17-CE24-0020) and the IDEX-LYON from Université de Lyon, Scientific Breakthrough project TORE within the Programme Investissements d’Avenir (ANR-19-IDEX-0005). He is also supported by the Auvergne-Rhône-Alpes region in the framework of PAI2020 and the Vingroup Innovation Foundation (VINIF) annual research grant program under Project Code VINIF.2021.DA00169. H.C.N. acknowledges the Deutsche Forschungsgemeinschaft (DFG, German

Research Foundation, project numbers 447948357 and 440958198), the Sino-German Center for Research Promotion (Project M-0294), and the ERC (Consolidator Grant 683107/TempoQ). This research is funded in part by the Gordon and Betty Moore Foundation's EPIQS Initiative, grant GBMF9615 to L.P., and by the National Science Foundation MRSEC grant DMR 2011750 to Princeton University. Work at the Molecular Foundry is supported by the Office of Science, Office of Basic Energy Sciences, of the U.S. Department of Energy under Contract No. DE-AC02-05CH11231. We thank Scott Dhuey for assistance with electron beam lithography and Paolo Cazzato for the technical support.

V. AUTHOR CONTRIBUTION STATEMENT

AG performed the experiments and the data analysis with the support of MET and VA. HS, VA and AG edited the manuscript with the input of all the authors. LNP, KWB, and FR fabricated and post processed the sample. HS, HSN and HCN provided the theoretical framework and reproduced the experimental results through numerical simulation. DT and MDG provided insight on the physical processes and helped in the data interpretation. DT provided the code to control the setup. DB and DS supervised the work.

VI. COMPETING INTERESTS STATEMENT

The authors declare no competing interests.

VII. DATA AVAILABILITY STATEMENT

The raw experimental data and the code used in this study are available from the corresponding author upon reasonable request.

VIII. METHODS

A. Sample and experiment

A 500 nm thick $\text{Al}_{0.4}\text{Ga}_{0.6}\text{As}$ planar waveguide embedded with 12 GaAs quantum wells, 20 nm thick and spaced apart by 20 nm serves as the sample for our experiments [16, 39, 61], the resulting exciton transitions are investigated in Fig. S6. The waveguide heterostructure is etched over an $300 \times 50 \mu\text{m}$ area along the x and y direction, respectively, such to possess a one-dimensional (1D) grating along the x -direction. Several replicas of the grating are etched on the sample with slightly different periods and filling factors, in order to finely tune the dispersion properties [39], refer to Fig. S7 for the effect of the grating pitch on to the polariton dispersion.

It is important to note that an ideal BIC state can only exist in infinite structures. However, the finite size of the grating and the strong coupling with the excitonic transition impose an upper limit on the BIC lifetime, effectively resulting in the polariton BIC being a quasi-BIC state. A quantitative estimation of the quality factor can be found in Section S8 and S9 of the Supplemental Material.

In order to prevent exciton dissociation and maintain strong light-matter coupling, the sample is cooled to 4 K during the experiment using a closed loop helium cryostat. The excitation is performed non-resonantly using an 80 Mhz, fs pulsed laser at 770 nm wavelength. The laser profile focused on the sample is precisely shaped with a spatial light modulator. A feedback method on the collected PL from the sample is employed to ensure uniformity across multiple spots [62]. The spot size for all the results displayed in this manuscript is set to $6.5 \mu\text{m}$ full-width-at-half-maximum (FWHM). All results in the study are extracted along the center of the waveguide (i.e., along k_x at $k_y = 0$).

We note that despite the effective attractive pull of the pump spot onto the polaritons the real space PL in Fig. 1e extends much further, $\approx 20 \mu\text{m}$, than the $6.5 \mu\text{m}$ FWHM of the excitation spot (see Fig. S10). This is due to the enhanced diffusion of excitons sustaining the condensate which obtain a larger group velocity in the strong coupling regime.

B. Modeling

Polaritons in our systems are dictated by the Dirac Hamiltonian (1) in the basis of counter-propagating polaritons of group velocity $\pm v$. The Hamiltonian includes the diffractive coupling of strength U , the radiative loss/coupling of strength γ and the potential $V(x)$ from the excitonic reservoir that is induced by the structured optical pump. For multispot excitation configuration of N spots focused at $x_{j=1..N}$, each spot induces a Gaussian potential of height V_0 and waist w . The potential $V(x)$ is then given by $V(x) = V_0 \sum_{j=1}^N e^{-(x-x_j)^2/2w^2}$.

For all theoretical calculations we use $w = 8.5 \mu\text{m}$ corresponding to $20 \mu\text{m}$ FWHM trap size. This trap size value is extracted from the real-space photoluminescence measurement (see Fig. S5 in the Supplemental Information). As explained previously the larger trap size with respect to the pump $6.5 \mu\text{m}$ FWHM is due to the finite diffusion of low-momentum excitons from the pump spot which gain substantial group velocity in the strong coupling regime. The loss parameter is taken as $\gamma = 0.153$ meV based on past results [16]. The values of U and v are directly extracted from the polariton dispersion below threshold exhibiting a band gap of $2U$ and curvature $\pm \frac{v^2}{2U}$ (see Fig. S1 in the Supplemental Information for measured dispersions below threshold). The experimental measurement have been performed on three grating structures having three different detuning: Grat-

ing 1 ($U = 0.7$ meV, $v = 32 \mu\text{m ps}^{-1}$) for single trapped BIC condensate experiment, Grating 2 ($U = 1.2$ meV, $v = 42 \mu\text{m ps}^{-1}$) for BIC polariton molecules experiment and Grating 3 ($U = 0.4$ meV, $v = 24 \mu\text{m ps}^{-1}$) for BIC condensate chains. Therefore, the only fitting parameter for all theoretical calculation is $V_0 = 3.5$ meV.

The calculated dispersions in Figs. 1d,e and Fig. 4b were obtained by averaging over the dynamics of multiple random initial conditions in (1) (i.e., Monte-Carlo sampling) that were weighted by the pump profile $V(x)$. The depletion seen around $k_x \approx 0$ in the simulated PL in Fig. 1(e) can be attributed to the resonant coupling of blueshifted low momentum fluctuations in the

upper branch to $k > 0$ momentum states. The energy of molecule states in Fig. 2g and their profiles in Fig. 2c-f and Fig. 4b,c are obtained by numerically solving the bound state solutions of the Dirac equation (1). Specifically, the obtained near-field profiles (in both real and momentum space) are converted into far-field profiles by suppressing the Fourier components corresponding to guided modes below the light cone. Finally, the polarization patterns in Fig. 4d,e are calculated from the spinor components of the Dirac equation solutions. Detailed theoretical framework for Dirac polaritons will be discussed elsewhere.

-
- [1] C. W. Hsu, B. Zhen, A. D. Stone, J. D. Joannopoulos, and M. Soljačić, Bound states in the continuum, *Nature Reviews Materials* **1**, 16048 (2016).
 - [2] S. I. Azzam and A. V. Kildishev, Photonic bound states in the continuum: From basics to applications, *Advanced Optical Materials* **9**, 2001469 (2021).
 - [3] A. Kodigala, T. Lepetit, Q. Gu, B. Bahari, Y. Fainman, and B. Kanté, Lasing action from photonic bound states in continuum, *Nature* **541**, 196 (2017).
 - [4] M.-S. Hwang, H.-C. Lee, K.-H. Kim, K.-Y. Jeong, S.-H. Kwon, K. Koshelev, Y. Kivshar, and H.-G. Park, Ultralow-threshold laser using super-bound states in the continuum, *Nature Communications* **12**, 4135 (2021).
 - [5] B. Zhen, C. W. Hsu, L. Lu, A. D. Stone, and M. Soljačić, Topological nature of optical bound states in the continuum, *Phys. Rev. Lett.* **113**, 257401 (2014).
 - [6] H. M. Doleman, F. Monticone, W. den Hollander, A. Alù, and A. F. Koenderink, Experimental observation of a polarization vortex at an optical bound state in the continuum, *Nature Photonics* **12**, 397 (2018).
 - [7] H. Chen, H. Wang, K. Yin Wong, and D. Lei, High-q localized surface plasmon resonance based on bound states in the continuum for enhanced refractive index sensing, *Opt. Lett.* **47**, 609 (2022).
 - [8] J. M. Foley, S. M. Young, and J. D. Phillips, Symmetry-protected mode coupling near normal incidence for narrow-band transmission filtering in a dielectric grating, *Phys. Rev. B* **89**, 165111 (2014).
 - [9] A. Aigner, A. Tittl, J. Wang, T. Weber, Y. Kivshar, S. A. Maier, and H. Ren, *Plasmonic bound states in the continuum to tailor light-matter coupling* (2022).
 - [10] S. D. Krasikov, A. A. Bogdanov, and I. V. Iorsh, Nonlinear bound states in the continuum of a one-dimensional photonic crystal slab, *Phys. Rev. B* **97**, 224309 (2018).
 - [11] D. Dolina and A. Yulin, Interactions of the solitons in periodic driven-dissipative systems supporting quasi-bound states in the continuum, *Phys. Rev. E* **104**, 054214 (2021).
 - [12] L. Lu, Q. Le-Van, L. Ferrier, E. Drouard, C. Seassal, and H. S. Nguyen, Engineering a light-matter strong coupling regime in perovskite-based plasmonic metasurface: quasi-bound state in the continuum and exceptional points, *Photon. Res.* **8**, A91 (2020).
 - [13] V. Kravtsov, E. Khestanova, F. A. Benimetskiy, T. Ivanova, A. K. Samusev, I. S. Sinev, D. Pidgayko, A. M. Mozharov, I. S. Mukhin, M. S. Lozhkin, Y. V. Kapitonov, A. S. Brichkin, V. D. Kulakovskii, I. A. Shelykh, A. I. Tartakovskii, P. M. Walker, M. S. Skolnick, D. N. Krizhanovskii, and I. V. Iorsh, Nonlinear polaritons in a monolayer semiconductor coupled to optical bound states in the continuum, *Light: Science & Applications* **9**, 56 (2020).
 - [14] N. H. M. Dang, S. Zanotti, E. Drouard, C. Chevalier, G. Trippé-Allard, M. Amara, E. Deleporte, V. Ardizzone, D. Sanvitto, L. C. Andreani, C. Seassal, D. Gerace, and H. S. Nguyen, Realization of Polaritonic Topological Charge at Room Temperature Using Polariton Bound States in the Continuum from Perovskite Metasurface, *Advanced Optical Materials* **10**, 2102386 (2022).
 - [15] T. Byrnes, N. Y. Kim, and Y. Yamamoto, Exciton-polariton condensates, *Nature Physics* **10**, 803 (2014).
 - [16] V. Ardizzone, F. Riminucci, S. Zanotti, A. Gianfrate, M. Efthymiou-Tsironi, D. G. Suàrez-Forero, F. Todisco, M. De Giorgi, D. Trypogeorgos, G. Gigli, K. Baldwin, L. Pfeiffer, D. Ballarini, H. S. Nguyen, D. Gerace, and D. Sanvitto, Polariton Bose-Einstein condensate from a bound state in the continuum, *Nature* **605**, 447 (2022).
 - [17] H. Deng, H. Haug, and Y. Yamamoto, Exciton-polariton bose-einstein condensation, *Rev. Mod. Phys.* **82**, 1489 (2010).
 - [18] C. Ciuti, V. Savona, C. Piermarocchi, A. Quattropani, and P. Schwendimann, Role of the exchange of carriers in elastic exciton-exciton scattering in quantum wells, *Phys. Rev. B* **58**, 7926 (1998).
 - [19] S. Klembt, T. H. Harder, O. A. Egorov, K. Winkler, R. Ge, M. A. Bandres, M. Emmerling, L. Worschech, T. C. H. Liew, M. Segev, C. Schneider, and S. Höfling, Exciton-polariton topological insulator, *Nature* **562**, 552 (2018).
 - [20] D. Sanvitto, F. M. Marchetti, M. H. Szymańska, G. Tosi, M. Baudisch, F. P. Laussy, D. N. Krizhanovskii, M. S. Skolnick, L. Marrucci, A. Lemaître, J. Bloch, C. Tejedor, and L. Viña, Persistent currents and quantized vortices in a polariton superfluid, *Nature Physics* **6**, 527 (2010).
 - [21] N. G. Berloff, M. Silva, K. Kalinin, A. Askitopoulos, J. D. Töpfer, P. Cilibrizzi, W. Langbein, and P. G. Lagoudakis, Realizing the classical xy hamiltonian in polariton simulators, *Nature Materials* **16**, 1120 (2017).
 - [22] R. Tao, K. Peng, L. Haeberlé, Q. Li, D. Jin, G. R. Fleming, S. Kéna-Cohen, X. Zhang, and W. Bao, Halide per-

- ovskites enable polaritonic xy spin hamiltonian at room temperature, *Nature Materials* **21**, 761 (2022).
- [23] H. Ohadi, A. J. Ramsay, H. Sigurdsson, Y. del Valle-Inclan Redondo, S. I. Tsintzos, Z. Hatzopoulos, T. C. H. Liew, I. A. Shelykh, Y. G. Rubo, P. G. Savvidis, and J. J. Baumberg, Spin order and phase transitions in chains of polariton condensates, *Phys. Rev. Lett.* **119**, 067401 (2017).
- [24] C. Schneider, K. Winkler, M. D. Fraser, M. Kamp, Y. Yamamoto, E. A. Ostrovskaya, and S. Höfling, Exciton-polariton trapping and potential landscape engineering, *Reports on Progress in Physics* **80**, 016503 (2016).
- [25] A. Amo and J. Bloch, Exciton-polaritons in lattices: A non-linear photonic simulator, *Comptes Rendus Physique* **17**, 934 (2016), polariton physics / Physique des polaritons.
- [26] A. Kavokin, T. C. H. Liew, C. Schneider, P. G. Lagoudakis, S. Klemmt, and S. Höfling, Polariton condensates for classical and quantum computing, *Nature Reviews Physics* **4**, 435 (2022).
- [27] M. Galbiati, L. Ferrier, D. D. Solnyshkov, D. Tanese, E. Wertz, A. Amo, M. Abbarchi, P. Senellart, I. Sagnes, A. Lemaître, E. Galopin, G. Malpuech, and J. Bloch, Polariton condensation in photonic molecules, *Phys. Rev. Lett.* **108**, 126403 (2012).
- [28] R. I. Kaitouni, O. El Daïf, A. Baas, M. Richard, T. Paraiso, P. Lugan, T. Guillet, F. Morier-Genoud, J. D. Ganière, J. L. Staehli, V. Savona, and B. Deveaud, Engineering the spatial confinement of exciton polaritons in semiconductors, *Phys. Rev. B* **74**, 155311 (2006).
- [29] R. Jayaprakash, C. E. Whittaker, K. Georgiou, O. S. Game, K. E. McGhee, D. M. Coles, and D. G. Lidzey, Two-dimensional organic-exciton polariton lattice fabricated using laser patterning, *ACS Photonics* **7**, 2273 (2020).
- [30] N. Y. Kim, K. Kusudo, C. Wu, N. Masumoto, A. Löf- fler, S. Höfling, N. Kumada, L. Worschech, A. Forchel, and Y. Yamamoto, Dynamical d-wave condensation of exciton-polaritons in a two-dimensional square-lattice potential, *Nature Physics* **7**, 681 (2011).
- [31] E. Wertz, L. Ferrier, D. D. Solnyshkov, R. Johne, D. Sanvitto, A. Lemaître, I. Sagnes, R. Grousson, A. V. Kavokin, P. Senellart, G. Malpuech, and J. Bloch, Spontaneous formation and optical manipulation of extended polariton condensates, *Nature Physics* **6**, 860 (2010).
- [32] S. Alyatkin, H. Sigurdsson, A. Askitopoulos, J. D. Töpfer, and P. G. Lagoudakis, Quantum fluids of light in all-optical scatterer lattices, *Nature Communications* **12**, 5571 (2021).
- [33] P. Cristofolini, A. Dreismann, G. Christmann, G. Franchetti, N. G. Berloff, P. Tsotsis, Z. Hatzopoulos, P. G. Savvidis, and J. J. Baumberg, Optical superfluid phase transitions and trapping of polariton condensates, *Phys. Rev. Lett.* **110**, 186403 (2013).
- [34] A. Askitopoulos, H. Ohadi, A. V. Kavokin, Z. Hatzopoulos, P. G. Savvidis, and P. G. Lagoudakis, Polariton condensation in an optically induced two-dimensional potential, *Phys. Rev. B* **88**, 041308 (2013).
- [35] L. Pickup, H. Sigurdsson, J. Ruostekoski, and P. G. Lagoudakis, Synthetic band-structure engineering in polariton crystals with non-hermitian topological phases, *Nature Communications* **11**, 4431 (2020).
- [36] M. Pieczarka, E. Estrecho, S. Ghosh, M. Wurdack, M. Steger, M. Steger, D. W. Snoke, K. West, L. N. Pfeiffer, T. C. H. Liew, A. G. Truscott, E. A. Ostrovskaya, and E. A. Ostrovskaya, Topological phase transition in an all-optical exciton-polariton lattice, *Optica* **8**, 1084 (2021).
- [37] F. Baboux, D. D. Bernardis, V. Goblot, V. N. Gladilin, C. Gomez, E. Galopin, L. L. Gratiet, A. Lemaître, I. Sagnes, I. Carusotto, M. Wouters, A. Amo, and J. Bloch, Unstable and stable regimes of polariton condensation, *Optica* **5**, 1163 (2018).
- [38] D. Tanese, H. Flayac, D. Solnyshkov, A. Amo, A. Lemaître, E. Galopin, R. Braive, P. Senellart, I. Sagnes, G. Malpuech, and J. Bloch, Polariton condensation in solitonic gap states in a one-dimensional periodic potential, *Nature Communications* **4**, 1749 (2013), number: 1 Publisher: Nature Publishing Group.
- [39] F. Riminucci, V. Ardizzone, L. Francaviglia, M. Lorenzon, C. Stavarakas, S. Dhuey, A. Schwartzberg, S. Zanotti, D. Gerace, K. Baldwin, L. N. Pfeiffer, G. Gigli, D. F. Ogletree, A. Weber-Bargioni, S. Cabrini, and D. Sanvitto, Nanostructured GaAs/(Al,Ga)As waveguide for low-density polariton condensation from a bound state in the continuum, *Phys. Rev. Applied* **18**, 024039 (2022).
- [40] Note that two other polariton branches exist above the exciton energy [12] but are weakly populated and not relevant to this study.
- [41] R. Gati and M. K. Oberthaler, A bosonic Josephson junction, *Journal of Physics B: Atomic, Molecular and Optical Physics* **40**, R61 (2007).
- [42] K. G. Lagoudakis, B. Pietka, M. Wouters, R. André, and B. Deveaud-Plédran, Coherent oscillations in an exciton-polariton Josephson junction, *Phys. Rev. Lett.* **105**, 120403 (2010).
- [43] M. Abbarchi, A. Amo, V. G. Sala, D. D. Solnyshkov, H. Flayac, L. Ferrier, I. Sagnes, E. Galopin, A. Lemaître, G. Malpuech, and J. Bloch, Macroscopic quantum self-trapping and Josephson oscillations of exciton polaritons, *Nature Physics* **9**, 275 (2013).
- [44] C. Kurtzschid, D. Dung, E. Busley, F. Vewinger, A. Rosch, and M. Weitz, Thermally condensing photons into a coherently split state of light, *Science* **366**, 894 (2019).
- [45] P. E. Allain and J. N. Fuchs, Klein tunneling in graphene: optics with massless electrons, *The European Physical Journal B* **83**, 301 (2011).
- [46] M. A. Khamsehchi, K. Hossain, M. E. Mossman, Y. Zhang, T. Busch, M. M. Forbes, and P. Engels, Negative-mass hydrodynamics in a spin-orbit-coupled Bose-Einstein condensate, *Phys. Rev. Lett.* **118**, 155301 (2017).
- [47] M. Wurdack, T. Yun, M. Katzer, A. G. Truscott, A. Knorr, M. Selig, E. A. Ostrovskaya, and E. Estrecho, Negative-mass exciton polaritons induced by dissipative light-matter coupling in an atomically thin semiconductor, *Nature Communications* **14**, 1026 (2023).
- [48] F. Schäfer, T. Fukuhara, S. Sugawa, Y. Takasu, and Y. Takahashi, Tools for quantum simulation with ultracold atoms in optical lattices, *Nature Reviews Physics* **2**, 411 (2020).
- [49] M. J. Hartmann, F. G. S. L. Brandão, and M. B. Plenio, Strongly interacting polaritons in coupled arrays of cavities, *Nature Physics* **2**, 849 (2006).
- [50] P. St-Jean, V. Goblot, E. Galopin, A. Lemaître, T. Ozawa, L. Le Gratiet, I. Sagnes, J. Bloch, and A. Amo, Lasing in topological edge states of a one-dimensional lat-

- tice, *Nature Photonics* **11**, 651 (2017).
- [51] J. Ni, C. Huang, L.-M. Zhou, M. Gu, Q. Song, Y. Kivshar, and C.-W. Qiu, Multidimensional phase singularities in nanophotonics, *Science* **374**, eabj0039 (2021).
 - [52] M. Atala, M. Aidelsburger, J. T. Barreiro, D. Abanin, T. Kitagawa, E. Demler, and I. Bloch, Direct measurement of the zak phase in topological bloch bands, *Nature Physics* **9**, 795 (2013).
 - [53] L. Lu, L. Fu, J. D. Joannopoulos, and M. Soljačić, Weyl points and line nodes in gyroid photonic crystals, *Nature Photonics* **7**, 294 (2013).
 - [54] Y. Li, C. T. Chan, and E. Mazur, Dirac-like cone-based electromagnetic zero-index metamaterials, *Light: Science & Applications* **10**, 203 (2021).
 - [55] M. Król, I. Septembre, P. Oliwa, M. Kędziora, K. Łempicka-Mirek, M. Muszyński, R. Mazur, P. Morawiak, W. Piecek, P. Kula, W. Bardyszewski, P. G. Lagoudakis, D. D. Solnyshkov, G. Malpuech, B. Piętka, and J. Szczytko, Annihilation of exceptional points from different dirac valleys in a 2d photonic system, *Nature Communications* **13**, 5340 (2022).
 - [56] M. Milićević, G. Montambaux, T. Ozawa, O. Jamadi, B. Real, I. Sagnes, A. Lemaître, L. Le Gratiet, A. Harouri, J. Bloch, and A. Amo, Type-iii and tilted dirac cones emerging from flat bands in photonic orbital graphene, *Phys. Rev. X* **9**, 031010 (2019).
 - [57] L. Polimeno, A. Fieramosca, G. Lerario, L. D. Marco, M. D. Giorgi, D. Ballarini, L. Dominici, V. Ardizzone, M. Pugliese, C. T. Prontera, V. Maiorano, G. Gigli, C. Leblanc, G. Malpuech, D. D. Solnyshkov, and D. Sanvitto, Experimental investigation of a non-abelian gauge field in 2D perovskite photonic platform, *Optica* **8**, 1442 (2021).
 - [58] R. Jackiw and C. Rebbi, Solitons with fermion number $\frac{1}{2}$, *Phys. Rev. D* **13**, 3398 (1976).
 - [59] T. X. Tran and F. Biancalana, Linear and nonlinear photonic Jackiw-Rebbi states in interfaced binary waveguide arrays, *Phys. Rev. A* **96**, 013831 (2017).
 - [60] K. Y. Lee, K. W. Yoo, Y. Choi, G. Kim, S. Cheon, J. W. Yoon, and S. H. Song, Topological guided-mode resonances at non-hermitian nanophotonic interfaces, *Nanophotonics* **10**, 1853 (2021).
 - [61] D. G. Suárez-Forero, F. Riminucci, V. Ardizzone, M. D. Giorgi, L. Dominici, F. Todisco, G. Lerario, L. N. Pfeiffer, G. Gigli, D. Ballarini, and D. Sanvitto, Electrically controlled waveguide polariton laser, *Optica* **7**, 1579 (2020).
 - [62] J. D. Töpfer, I. Chatzopoulos, H. Sigurdsson, T. Cookson, Y. G. Rubo, and P. G. Lagoudakis, Engineering spatial coherence in lattices of polariton condensates, *Optica* **8**, 106 (2021).